Available online at www.sciencedirect.com
ScienceDirect
Acta Materialia 59 (2011) 5276–5287
Acta MATERIALIA
www.elsevier.com/locate/actamat

Reaction in Ni–Al laminates by laser-shock compression and spalling

C.T. Wei [a,*], B.R. Maddox [b], A.K. Stover [c], T.P. Weihs [c], V.F. Nesterenko [a], M.A. Meyers [a]

[a] University of California, San Diego, La Jolla, CA 92093-0411, USA
[b] Lawrence Livermore National Laboratory, Livermore, CA 94551, USA
[c] Johns Hopkins University, Baltimore, MD 21218, USA

Received 16 September 2010; received in revised form 29 April 2011; accepted 1 May 2011
Available online 12 June 2011

Abstract

Reactive Ni/Al laminates (with bilayer thicknesses of 5 and 30 μm) were subjected to direct high-intensity laser shock-wave loading. The laser intensity was varied between $\sim 2.68 \times 10^{11}$ and $\sim 1.28 \times 10^{13}$ W cm^{-2}, with two distinct initial pulse durations: 3 and 8 ns. Analytical and computational estimations (HYADES) were conducted to simulate the propagation of the shock wave and obtain the initial shock pressure. The thinner bilayer laminate exhibited intense localized interfacial reaction at the higher laser intensity (1.28×10^{13} W cm^{-2}), but the intermetallic reaction did not propagate through the laminates. The estimated temperature changes inside the sample, cooling rate, and cooling time were calculated by analyzing the intermetallic dendrites. Scanning electron microscopy, electron-dispersive spectroscopy and X-ray diffraction were carried out for identifying the compositions of intermetallic products. Increase in the duration of laser shock wave enhanced the reaction in laminates. It is demonstrated that the methodology of laser shock is suited to investigate the threshold conditions for dynamic mechanical reaction initiation.
© 2011 Acta Materialia Inc. Published by Elsevier Ltd. All rights reserved.

Keywords: Shock-induced reactions; Laser; Aluminum; Nickel; Intermetallics

1. Introduction

Shock- and shear-induced exothermic chemical reactions have been the subject of intense study because of their possible use to synthesize novel materials [1–6]. More recently, the potential of dynamically initiated exothermic reactions is being investigated for controlling energy release processes in ballistic applications [7]. Their potential uses in shell casings, by augmenting the kinetic energy with the chemical energy, are attractive.

Reactive laminates have found numerous applications in joining metals [8–11], assembling electronic devices [12], and providing localized heat sources for bonding components [13]. The laminates have a well-ordered meso-structure and the exothermic reaction can be tailored by incorporating other elements or manipulating the thickness of the layers [14,15]. For these reasons, reactive laminates with different meso-structures have been chosen in this study to investigate dynamic reactions caused by a powerful laser source.

The Ni–Al system was selected because of the high exothermicity of reactions. The principal intermetallics in the Ni–Al system are NiAl, $NiAl_3$, Ni_2Al_3, and Ni_3Al [16–19], which have relatively low density, high strength, good oxidation resistance, and excellent thermal and electrical conductivity. These exothermic reactions release energy varying from 129.2 to 293.2 kJ mol^{-1} (150.6 kJ mol^{-1} $NiAl_3$, 293.2 kJ mol^{-1} Ni_2Al_3, and 129.2 kJ mol^{-1} NiAl) [20]. Since these energies significantly raise the temperature of the product, they may facilitate the self-propagating high temperature synthesis (SHS).

Conventional shock loading experiments have been traditionally conducted by planar flyer-plate impact [21–25] and direct high explosive detonation [26–30]. These methods generate shock waves with pressures of about few tens of GPa and relatively long pulse durations, usually of the order of 1–10 μs. Recently, high intensity lasers have been

* Corresponding author.
E-mail address: chwei@ucsd.edu (C.T. Wei).

1359-6454/$36.00 © 2011 Acta Materialia Inc. Published by Elsevier Ltd. All rights reserved.
doi:10.1016/j.actamat.2011.05.004

applied to access a higher regime of pressures (hundreds of GPa), strain rates ($\sim 10^{10}$ s^{-1}) [31], and shorter pulse durations (a few nanoseconds). These high intensity laser-induced shock waves are accompanied by local temperature rises, crater damage in the laser-illuminated surface, spalling in the back surface, plasma generation, and possible exothermic reactions [32]. The use of lasers may benefit investigations of high-speed reactions [33], extremely-high strain-rate deformation [34,35], and microstructural failure mechanisms [36].

2. Experimental methods

The laminates were made by cold rolling of alternately stacked Ni and Al sheets [37]. This process produces bilayer thicknesses that are considerably larger than sputter deposition, also used to process reactive laminates. The details of the original thicknesses of Ni and Al pure elemental sheets are listed in Table 1. The reductions in original thickness were ~85–90%. After cold rolling, the laminates, which had total thicknesses of 0.8–0.9 mm, were cross-sectioned and imaged to determine an average bilayer thickness using a lineal intercept method. Average bilayer thicknesses of 5 and 30 μm were determined for the two samples rolled as shown in Table 1; it can be seen that two starting thicknesses of Ni and Al were used.

Fig. 1a–d shows the morphologies of the cross-sections of the as-produced laminates with the two different bilayer thicknesses. The cross-sectional images of the thicker bilayer laminates were taken both longitudinally and transversely to the rolling direction as shown in Fig. 1a and b, respectively. There are some irregularities in the mesostructure due to the rolling process. The transverse section shows distinct shear bands running at an angle to the Ni and Al layers. These bands are due to shear localization, a common occurrence in high-strain deformation in rolling. The differences of the microstructural features along the longitudinal and transverse sections of the thinner (5 μm) bilayer laminate are indistinguishable (Fig. 1c and d).

The laser compression experiments were carried out in the Jupiter laser facility of Lawrence Livermore National Laboratory using the Janus laser, which is a Nd-glass laser with a 532 nm pulse width. The laser energies were varied from ~24 to ~440 J. The durations of laser pulses were 3 and 8 ns. The laser beam size was 1.12 mm^2 and had a square footprint. A face plate was used to smooth out spatial pressure variations. Laminates were cut into 5 × 5 mm squares and attached to two steel washers having a 10 mm outer diameter and 2.5 mm inner diameter. The associated conditions of the laser experiments are given in Table 2. The experimental setup is schematically shown in Fig. 2a.

Table 1
Sample conditions.

Sample	Original Ni thickness (μm)	Original Al thickness (μm)	Bilayer thickness (μm)	Total thickness (mm)	Number of bilayers
Ni–Al-5 μm	18	25	5 (±0.53)	0.85–0.9	~180
Ni–Al-30 μm	127	178	30 (±2.7)	0.8–0.85	~20

Table 2
Conditions of experiments.

Bilayer thickness	8 ns laser energy (J)	Intensity of 8 ns laser (W cm^{-2})	3 ns laser energy (J)	Intensity of 3 ns laser (W cm^{-2})
5 μm	229	$\sim 2.56 \times 10^{12}$	107	$\sim 3.18 \times 10^{12}$
			430	$\sim 1.28 \times 10^{13}$
30 μm	24	$\sim 2.68 \times 10^{11}$	105	$\sim 3.13 \times 10^{12}$
	409	$\sim 4.56 \times 10^{12}$	421	$\sim 1.25 \times 10^{13}$

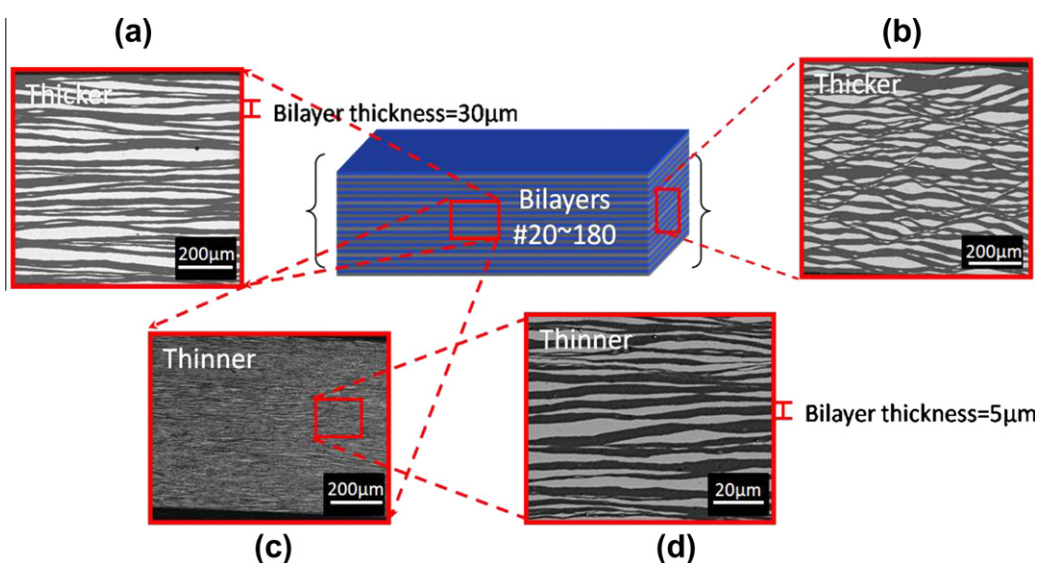

Fig. 1. Morphologies of sections of Ni–Al laminates (central schematic): (a) laminate with thicker (30 μm) bilayer; (b) laminate along longitudinal section; (c) laminate with thinner (5 μm) bilayer; (d) high magnification image of thinner bilayer.

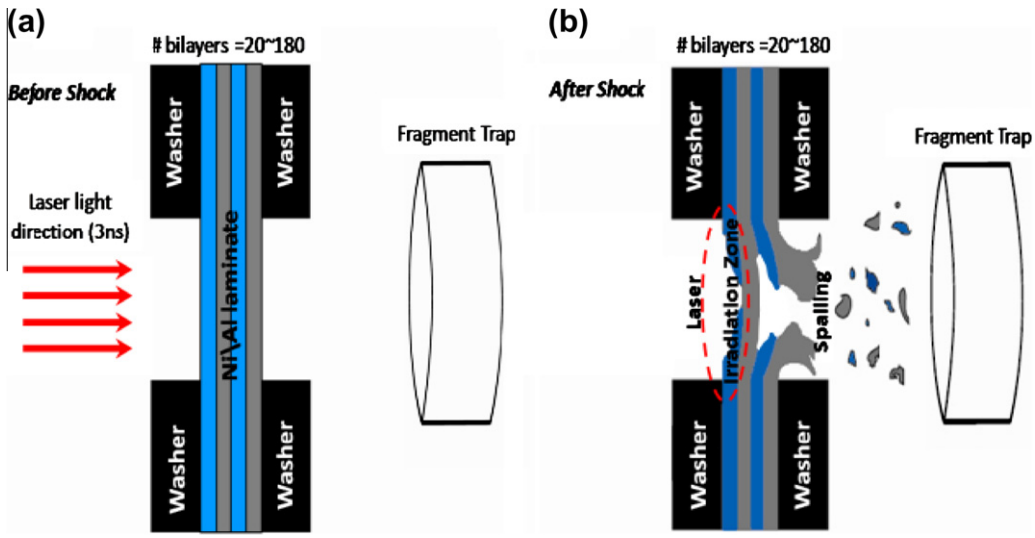

Fig. 2. Laser shock experimental setup: (a) sample placed between laser irradiation source and fragment trap, washers used to fix samples; (b) after laser irradiation, spall is formed and fragments are scattered from the spall surface and captured by fragment trap.

The geometry of sample after laser irradiation is schematically shown in Fig. 2b. The front surface (laser-exposed surface) shows a crater and the back surface exhibits a spall after the laser shock arrived and reflected from it. Fragments were captured by a fragment trap aligned with the sample. After laser irradiation, a Rigaku MiniFlex II diffraction unit was employed for analysis. A Philips XL30 environmental scanning electron microscope (SEM) equipped with an electron-dispersive spectrometer (EDS) was used to observe the cross-sections and morphologies of the samples.

3. Results

3.1. Estimate of laser shock-wave pressure in laminates

Two different methods were used to estimate the laser-induced shock-wave propagation in the laminates and to calculate the initial pressures.

The first method was to directly use Lindl's equation [38], which considers the pressure produced by laser shock as a strong function of laser intensity. The laser intensities in this study vary from $\sim 2.68 \times 10^{11}$ to $\sim 1.28 \times 10^{13}$ W cm^{-2}. The laser intensity I_{15} (in 10^{15} W cm^{-2}) can be translated into pressure P (in GPa) using:

$$P = 4 \times 10^3 \left(\frac{I_{15}}{\lambda}\right)^{\frac{2}{3}} \quad (1)$$

where λ is the wavelength of the laser pulse in micrometers. For laser energies of 100, 200, and 400 J with pulse durations of 3 and 8 ns, a spot area 1.12 mm^2, and a wavelength of laser equal to 532 nm, the initial pressures vary from 66.3 GPa to 321.3 GPa. The specific initial pressures are given in Table 3. This is a very approximate method, since no material parameters enter into it. The initial pressures are seen to be strongly related to the pulse duration, since the laser intensity is inversely proportional to the pulse duration: $I_{15} = \left(\frac{E(J)}{t(s) \times A(cm^2) \times 10^{15}}\right)$, where the E is the laser energy in J, t is the pulse duration in s, and A is the beam's cross-sectional area in cm^2. By considering the optical properties of Ni/Al, the reflectivity R (60%) [39] of materials can be incorporated into Lindl's equation using a modified equation:

$$P = 4 \times 10^3 \left(\frac{(1-R) \times I_{15}}{\lambda}\right)^{\frac{2}{3}} \quad (2)$$

The modified initial pressures are shown in Table 4. Tables 3 and 4 show that by increasing the laser duration to 8 ns, the laser intensity dramatically drops to nearly half of the value corresponding to 3 ns pulse duration at the same laser energy. Thus, the 8 ns laser experiments have a significantly decreased laser intensity while the duration of the thermal interaction is increased.

The second method is the computational prediction using the hydrodynamic code HYADES for characterization of laser shock propagation in materials. This radiation

Table 3
Initial pressures from Lindl's equation.

Laser energy (J)	Pressure (GPa) 3 ns	Pressure (GPa) 8 ns
100	127.5	66.3
200	202.4	105.2
400	321.3	167.1

Table 4
Initial pressures from modified Lindl's equation.

Laser energy (J)	Pressure (GPa) 3 ns	Pressure (GPa) 8 ns
100	68.4	35.6
200	108.6	56.5
400	172.4	89.7

hydrodynamic code provides a reasonable one-dimensional model for simulation of laser-induced shock-wave propagation. In order to simplify the simulation process, the strength parameters (strength and elastic modulus) were not introduced into this simulation. Fig. 3a shows shock propagation induced by the 400 J, 3 ns laser pulse through Ni–Al laminate, as compared to monolithic Al. The computation reveals that the pressure rises when the shock wave reaches the first Ni layer after passing through the Al layer. In a pure Al slab, a monotonic decay is observed (Fig. 3a, dash curves). The initial pressures in the first Ni layer obtained from simulation results for 100 and 400 J laser energies with 3 ns pulse duration are ~120 and ~300 GPa. The difference in shock impedances results in multiple reflections at interfaces (Fig. 3b) [39]. The shock wave enters the laminate through the Al layer (surface). It propagates through the Al layer to the adjacent Ni layer. From the Rankine–Hugoniot pressure–particle velocity curves of Ni and Al (in Fig. 3b), one can find the first transmitted shock from point 1 of the Al layer (incident shock in Al), corresponding to pressure P_1, to point 2 of the adjacent Ni layer, corresponding to pressure P_2. Along with the propagation of the shock wave in Ni/Al bilayers [39], the interfacial pressures can be estimated using the same pressure–particle velocity plots (Fig. 3b), following the sequence $1 \rightarrow 2 \rightarrow 3 \rightarrow 4 \rightarrow 5$. This reverberation sequence shows that as the shock front exits an Al layer and enters a Ni layer, the pressure increases (Fig. 3a from 1 to 2); the reverse occurs when the shock front enters an Al layer coming from a Ni layer (Fig. 3a from 2 to 3). This provides the rationale of the HYADES results. It should be mentioned that this procedure can be used only for relatively short shock waves; more complex situations need to be considered for long shock waves propagating in laminates [40,41]. Their impedance mismatch may cause the interfacial region of the nickel and the aluminum sheets to become more reactive.

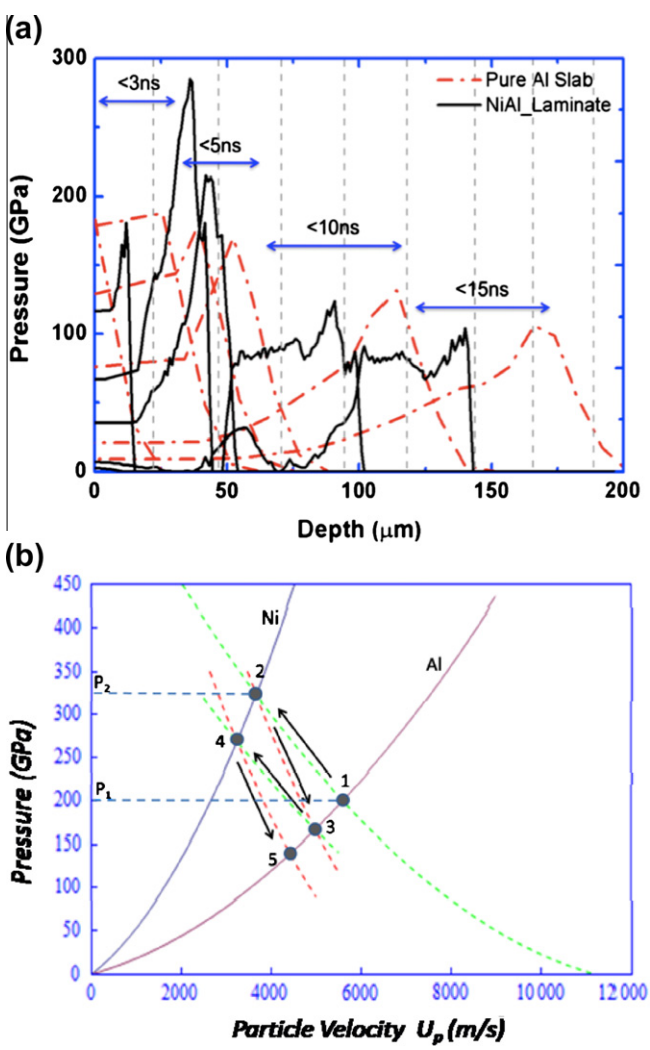

Fig. 3. Calculation of pressure pulse amplitude in Ni–Al: (a) laser shock wave (400 J; 3 ns) propagation in pure Al slab and laminate (HYADES Simulation); (b) Rankine–Hugoniot pressure vs. particle velocity plot for Ni and Al showing wave reflections.

These two calculational procedures provided the following consistent results:

- 3 ns, 100 J: 127.5 GPa (Lindl); 68.4 GPa (mod. Lindl); ~120 & 72 GPa (HYADES for Ni & Al)
- 3 ns, 400 J: 321 GPa (Lindl); 172.4 GPa (mod. Lindl); ~300 & 180 GPa (HYADES for Ni & Al)

It should be noted that the pressure in Al predicted by HYADES is lower because of its lower shock impedance. The initial pressures from the computational methods indicate that on the irradiated surface, the laser shock pressures exceed the pressure (3.5–5.4 GPa) of the intermetallic reaction barrier for the Ni + Al powder mixture reported by Eakins et al. [42]. This suggests that the laminates should have a certain amount of intermetallics in the recovered samples. However, the experimental results did not show intermetallics for some of the laser irradiated samples. The detailed analysis and possible explanations will be presented as follows.

3.2. Observation on fragments

The fragment-size dependence on bilayer thickness and laser shock energy is not analyzed in this work. It should be noted that the amount of debris is strongly related to the laser and sample conditions. The geometry of the fragments is not a critical aspect in this article. A detailed analysis of the fragmentation in vanadium under similar laser-shock loadings was developed [43]. Its application to the laminates is provided elsewhere [44].

The EDX dot-mapping images (insets of Fig. 4c) show that Ni (green[1] color) and Al (red color) layers are mixed in many areas of the thinner bilayer laminates after 400 J, 3 ns, laser irradiation. The SEM back-scattering electron

[1] For interpretation of color in Fig. 4, the reader is referred to the web version of this article.

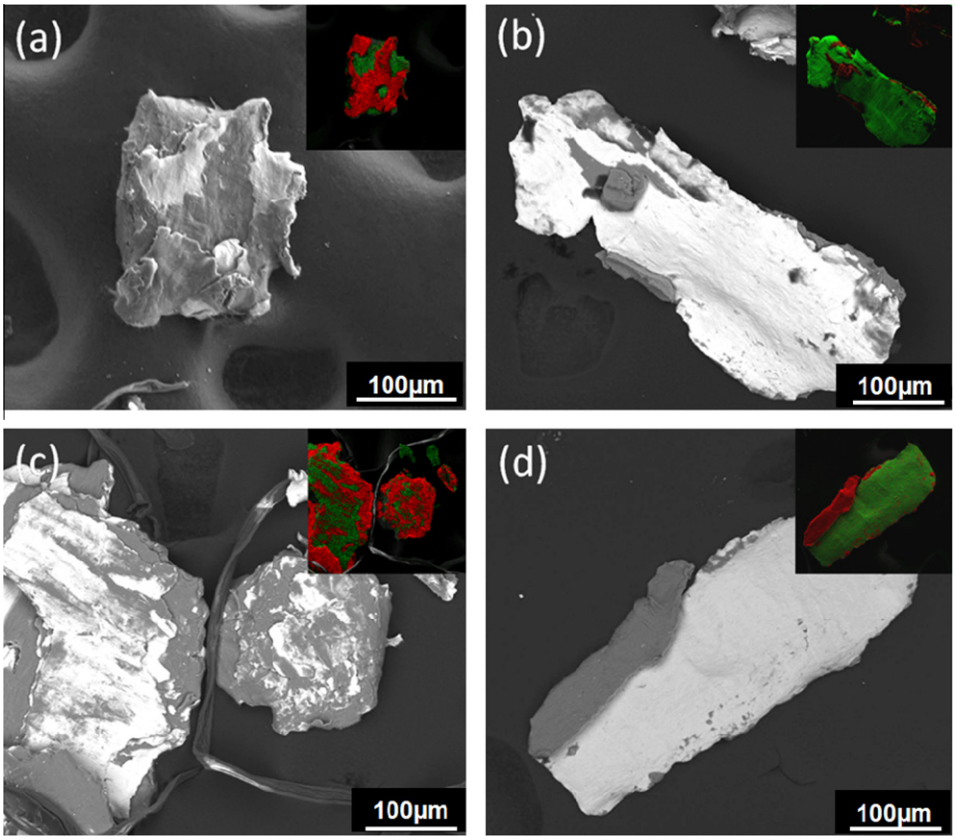

Fig. 4. Fragments from spall surface: (a) 5 μm and (b) 30 μm bilayer thickness (100 J 3 ns laser exposure); (c) 5 μm and (d) 30 μm bilayer thickness (400 J 3 ns laser exposure).

image (Fig. 4c) also provides apparent evidence that the Ni (bright part) disperses uniformly in the Al (gray part) matrix. Interestingly, except for the thinner bilayer recovered sample irradiated by 400 J, 3 ns laser, these samples do not show this intermixing phenomenon at the Ni/Al interface (Fig. 4a, b, d, and insets). This mixing might have occurred either before or following laser irradiation, due to the mechanical alloying mechanism from the cold-rolling process [45], or from the severe deformation of Ni and Al layers in spalling regions.

3.3. Surface morphologies

3.3.1. Laser experiments with 100 and 400 J, 3 ns

The morphologies of irradiated and spall surfaces were thoroughly inspected using an SEM with a back-scatter detector. The irradiated surfaces show cratering whereas the back surfaces show evidence of spalling. The irradiated and spall surfaces of the 30 μm laminate are shown in Fig. 5; the corresponding micrographs for the 5 μm laminate are shown in Fig. 6. The spall regions of 30 and 5 μm bilayer samples show no evidence of reaction, melting, or diffusion (Figs. 5b and d and 6b and d). Since the shock wave expanded radially in the materials, the spall regions are considerably larger than the laser beam size (1.12 mm^2); these are represented by dashed squares (Figs. 5 and 7). The bilayers were broken into metal strips and formed convex areas on the spall surfaces. The fragments of these strips were ejected and captured as debris (Fig. 3). It should be emphasized that no intermetallic reaction was found on the spall surface. This supports the observation of the fragmentation (Fig. 4b and d) in Section 3.2.

Recoiled strips of fractured laminar bilayers were found on the irradiated surfaces of thicker bilayer laminates due to their motion during spalling. These irradiated surfaces of the thinner bilayer samples had distinct macroscopic structures as compared to the thicker samples. The sample with 30 μm bilayer has fractured foils and rings marking vaporization (Fig. 5a and c).

The irradiated surfaces of thinner bilayer (5 μm) samples show significant melting on the laser-exposed regions (Fig. 6, insets in a and c). There are no peeled foils or fractured sheets on the surface, since the thinner bilayer sample does not have a continuous layer structure (Fig. 1c and d). The layer structures are broken up into segments due to the high strain ductile rolling. The microscopic morphologies on the irradiated surfaces of thinner bilayer samples show dendrites (Fig. 6a and c), which are identified as intermetallic compounds by EDX. Dendritic structures are widely distributed around the molten pool of the crater.

3.3.2. Laser experiments with 24, 229 and 409 J, 8 ns

By increasing the pulse duration at the same energy level, the intensity of laser was reduced; e.g. 400 J, 3 ns

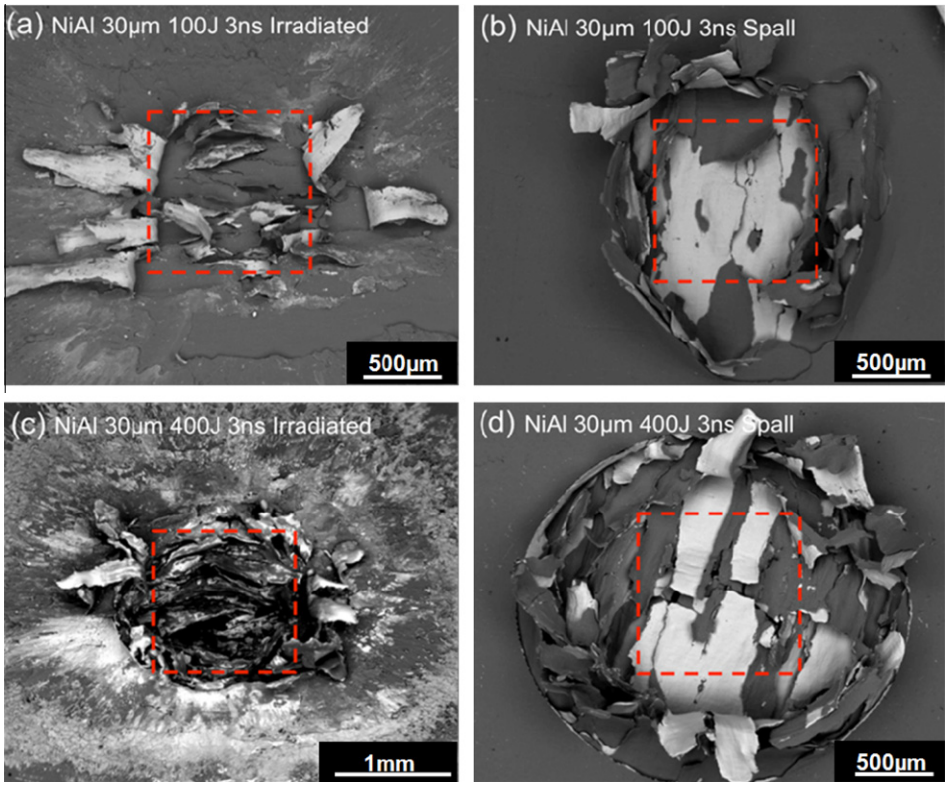

Fig. 5. SEM-BSE observations of samples with thicker bilayer (30 μm) exposed to (a and b) 100 J 3 ns and (c and d) 400 J 3 ns laser irradiation; (a and c) irradiated surface presenting melt, deposition from metal vaporization, and foil recoiling. Spall surfaces (b and d) revealed broken and peeled strips, without evidence of reaction.

laser has nearly three times higher intensity than 409 J, 8 ns laser (Table 2). Fig. 7a and c shows dendrites distributed on the irradiated surface of the 30 μm bilayer sample; these did not occur in the 3 ns laser pulse experiments. Dendrites are discovered, even in the 30 μm laminate with the lowest laser energy (24 J) exposure. The dendrites are also found on the thinner bilayer sample after 229 J (8 ns) laser exposure (Fig. 7e). As in the 3 ns experiments, these dendrites are distributed around the molten pools of the crater.

The microscopic characteristics of the spall areas after 8 ns laser irradiation were similar to the 3 ns laser experiments. On the spall surfaces, peeled foils and bent layers are seen, but no reaction is observed (Fig. 7f). The 8 ns laser experiments demonstrate that laser duration plays an important role on the reaction of the irradiated surfaces; nevertheless, neither the 24 nor 409 J laser energies are sufficient to propagate the reaction through the entire sample with the longer pulse duration.

The intermetallics formed at the 8 ns laser pulse duration experiments suggest that laser shock-assisted thermal reaction occurred intensively at the longer laser irradiation time [1,2]. In fact, for most of the laser shock experiments conducted on reactive materials, both laser shock-induced and laser shock-assisted thermal reactions coexisted and cannot be separated [1]. In order to discriminate between these two reaction mechanisms, the recovered samples were sectioned and characterized by SEM (Section 3.4).

3.4. Cross-sectional observations

Fig. 8a shows that intensive reaction took place in the thinner bilayer sample irradiated by 400 J, 3 ns laser. The reaction propagated into the sample to a depth of about 50 μm (~10 bilayers). This contrasts with Fig. 8b, the cross-sectional image at the edge of crater, suggesting that reaction did not propagate out of the crater area. It should be noted that the reaction was barely found on the cross-sections of samples with thicker bilayer after 3 ns laser pulse irradiation, which suggests that these laser irradiations were not sufficient to generate reaction in these samples. Increasing the pulse duration (8 ns) facilitated intermetallic reaction in the thicker bilayer sample (Fig. 8c); however, in the thinner bilayer (Fig. 8b), the intermetallic was barely detectable at the edge of the crater (Fig. 8d). These incompatible intermetallic phase formations in adjacent areas provide important hints as to the reaction mechanisms, which will be discussed in Section 4.3.

Intermetallic compounds formed along the interface of Ni–Al layers and grew into granular shapes in this study. The mechanism of intermetallic compound formation in shock compression was proposed by Meyers et al. [46,47]. The schematic sequence of Fig. 8e and the corresponding observation extracted from Fig. 8a, which is shown in Fig. 8f, provide a clear proof of each stage. The solid Al

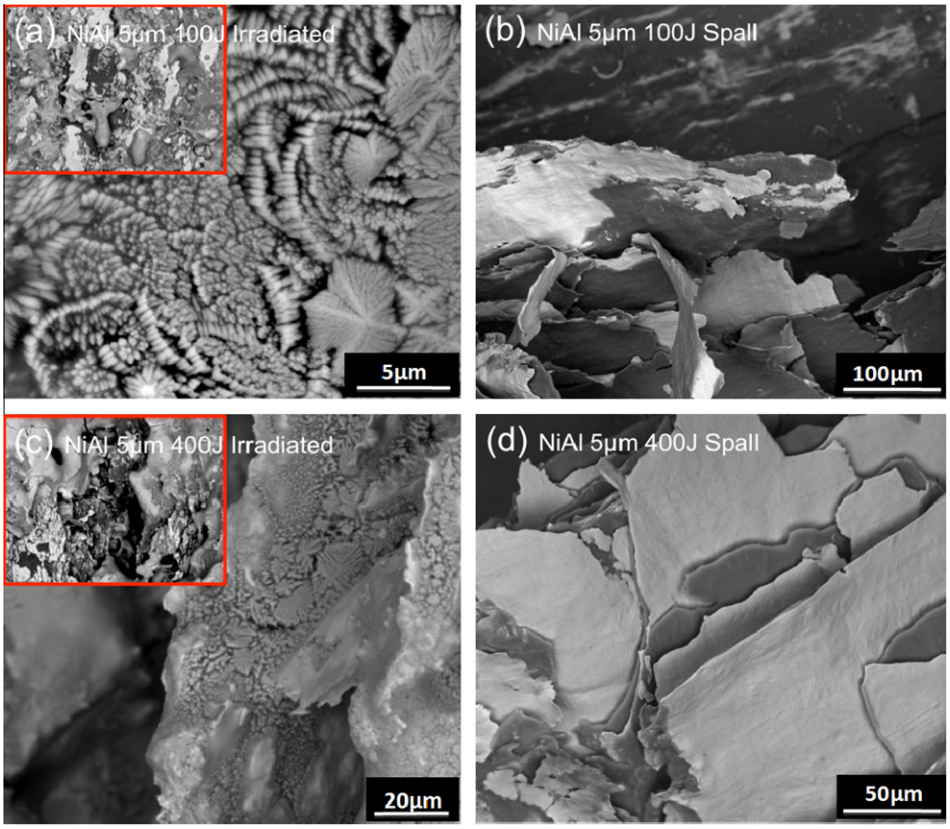

Fig. 6. SEM-BSE observations of samples with 5 μm bilayer irradiated at (a and b) 100 J 3 ns and (c and d) 400 J 3 ns laser; (a and c) dendrites, melt pools, and granules found on the irradiated surface. Fractures (b and d) observed on spall surfaces.

and Ni layers (Fig. 8e, step 1) represent the original state of the laminate. When laser shock compression is applied on the surface of laminates, the Al layer melts and initial intermetallic nucleation takes place at the interface of Ni/Al layers (Fig. 8e, step 2, and Fig. 8f, circle "a", respectively). After the reaction proceeds for a certain time, the intermetallic compounds agglomerate into spherules at the interface and turn elongated as they grow into elongated granules (Fig. 8e, step 3 and Fig. 8f, circle "b"), leading eventually to the formation of dendritic structures. As the granules reach a critical size, the neighboring spheres start to grow as well as to constrain the first spheres. These exert forces and expel the first grown granules. This forces the intermetallic compounds to disperse into the Al layer (Fig. 8e, step 4; Fig. 8f, circle "b"). These dispersed granules and dendrites might accumulate and cluster to become full dendrites (Fig. 8f, circle "c"). Notice that Fig. 8c shows the same sequence of reaction in the thicker bilayer sample as well, if the laser pulse duration is increased to 8 ns.

It should be noted that in the literature, the predicted shock-induced melting pressures of Ni and Al are ~275 and ~125 GPa respectively [48,49] and the corresponding melting temperatures are ~6400 and ~4750 K. These pressures are close to the estimated pressure on the laser irradiated surface (see Section 3.1) and thus create opportunity of melting under shock pressure. This temperature increase is incorporated into the thermal energy released by the reaction. Therefore, the reaction has a great opportunity to self-propagate into the adjacent layers and through the entire sample. However, the self-propagating reaction is not found in this study.

3.5. Analysis of reaction products

X-ray diffraction (XRD) and EDS analyses were used to investigate the components of the reaction products after laser irradiation. XRD was conducted on cross-sectional samples before and after laser irradiation. The results show that before laser irradiation (Fig. 9a and b), there is no evidence of intermetallic compounds generated during the cold-rolling process; only Al and Ni peaks were found. After laser irradiation, XRD results show that for 3 ns laser pulse duration only the thinner (5 μm) bilayer sample has strong intermetallic compound peaks after 400 J laser irradiation (Fig. 9a dashed circle). The intermetallic compound was identified as NiAl. This agrees with recent in situ studies of self-propagating reactions in Ni/Al multilayer foils [33,49–51]. In these in situ studies, NiAl was the first intermetallic to form, regardless of whether the initial average composition was Al- or Ni-rich. Gavens et al. [14] also postulated the bilayer thickness effect for the intermetallic reaction. As the duration of the laser pulse was increased to 8 ns with total energies of 24 and 409 J, the XRD results (Fig. 9b) reveal more extensive reaction,

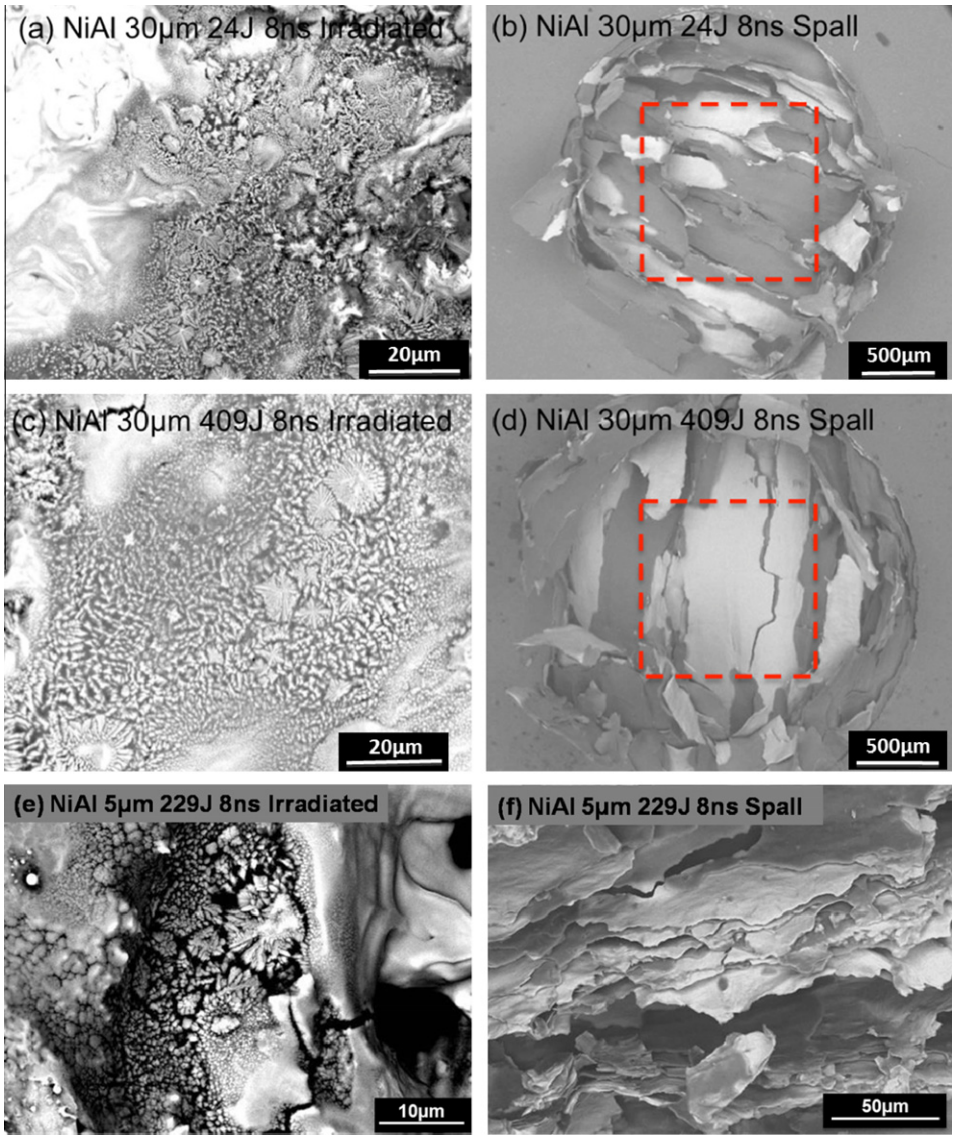

Fig. 7. 30 μm bilayer laminates (8 ns pulse duration): (a) 24 J irradiated surface; (b) 24 J spall surface; (c) 409 J irradiated; (d) 409 J spall. Both irradiated surfaces show reactions but none of the spall surfaces have reactions. (e) Ni/Al laminates with 5 μm bilayer subjected to 229 J, 8 ns laser pulse with 229 J: irradiated surface presents melts, dendrites, and granules. Clear evidence of reaction is shown. (f) no reaction on spall surface.

now for both thinner and thicker bilayer samples. This agrees with the previous microscopic cross-section observations (Figs. 5–7). In addition to the NiAl peaks, the possible Al-rich peaks of $NiAl_3$ were also found. Due to the high residual strain, fast reaction, and short heating time from laser irradiation, the Al-rich intermetallic, $NiAl_3$, has only three peaks in the XRD spectrum. No intermetallic compound is found by XRD for 24 J, 8 ns laser exposure on 30 μm bilayer sample (Fig. 9b). Thus, longer duration and higher laser energy benefit the laser shock reaction. This is consistent with the SEM observation of the irradiated surface (Fig. 7a). It suggests that longer duration of laser pulse is not always adequate for reaction if the laser energy is too low.

The EDX technique was also used in the analysis of the fragments and intermetallic dendrites. The EDX data show that the ratio of components in the dendrites vary from Ni:Al = 20:70 to Ni:Al = 19:81. Compared with the XRD analyses, which identify the intermetallic compounds as NiAl and $NiAl_3$, the EDX results show that those compounds are Al-rich phases. Due to the diagnostic spot size ~1 μm, and the electron scattering effect, the results of the EDX analysis of intermetallic compounds were always disturbed by the surrounding environment.

4. Discussion

The laser energy used in this study was approximately 10^4 times greater than the energy flux applied in conventional shock synthesis; however, surprisingly the reaction shown in the recovered samples was limited. Further discussions of the phase distributions of the pure Al and Ni,

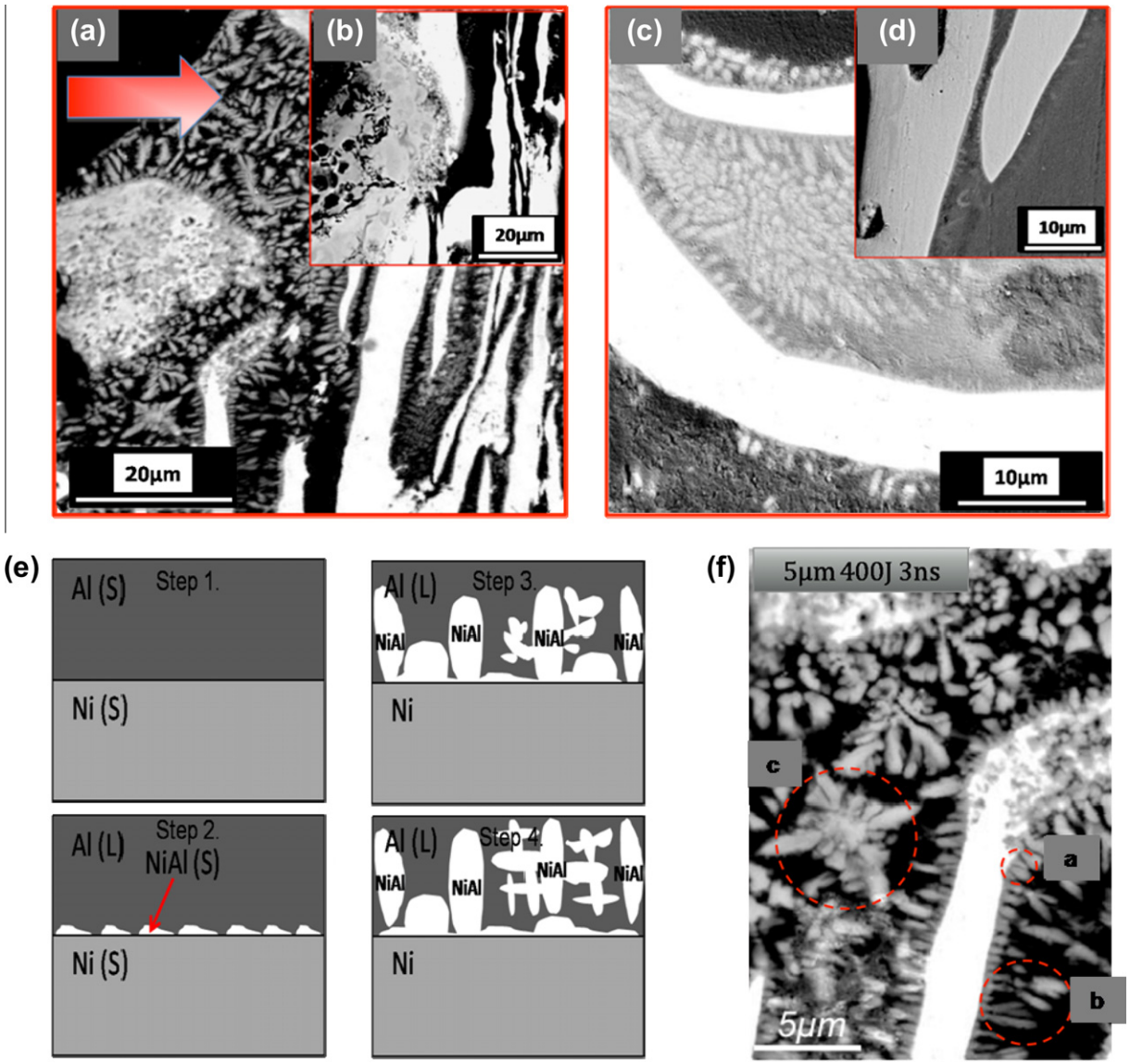

Fig. 8. Cross-sectional observations (SEM-BSE): (a) 5 μm bilayer laminate (400 J, 3 ns laser): dendrites were generated and found at 50 μm depth under the irradiated surface. (b) 5 μm bilayer laminates (400 J, 3 ns) at the edge of crater: It shows almost no intermetallic compound but still has the molten surface. (c) 30 μm bilayer laminate (400 J, 8 ns): intermetallic granules shown on the first and second bilayer (~35 μm depth). (d) 30 μm bilayer laminate (400 J, 8 ns) at the edge of crater: the dendrites dramatically disappear at the edge of the crater. (e) Schematic sequence of reaction and intermetallic compound formation. (f) The corresponding image for (e): circle "a" shows the granules formed by interfacial reaction; they grow, becoming elongated and are expelled from interface as shown in circle "b"; the expelled granules accumulate and grow to be fully dendritic structures as shown by circle "c".

intermetallic, and intermixing phases, on the recovered samples corresponding to the mechanisms are presented.

4.1. Fragmentation

Our estimates of pressures in the spall areas are higher than the reaction threshold for intermetallics, 3.5–4.5 GPa [42], at relatively longer shock durations (from milliseconds to several seconds). The absence of reaction in the fragments is probably due to the very short pulse duration (3 and 8 ns) of the laser shock and the relatively smaller plastic deformation in cold-rolled solid laminates compared to porous mixtures of powders in [42]. There is no experimental data for the threshold of intermetallic reactions at these pulse durations (3–8 ns). In this study, only the pure Al and Ni phases are presented in the fragments of the thicker bilayer samples (Fig. 4b and d). The fragments of thinner bilayer samples also have the Ni/Al intermixing phase (Fig. 4a and c), which was presented in Section 3.2.

4.2. Phase distributions in craters and spalls

The reaction products on irradiated surfaces, corresponding to laser shock pressures ~100 to ~300 GPa, show that laser energy induces an increase in temperature greater than the melting point of Al. The extent of intermetallic formation was greater in the 5 μm bilayer samples, which

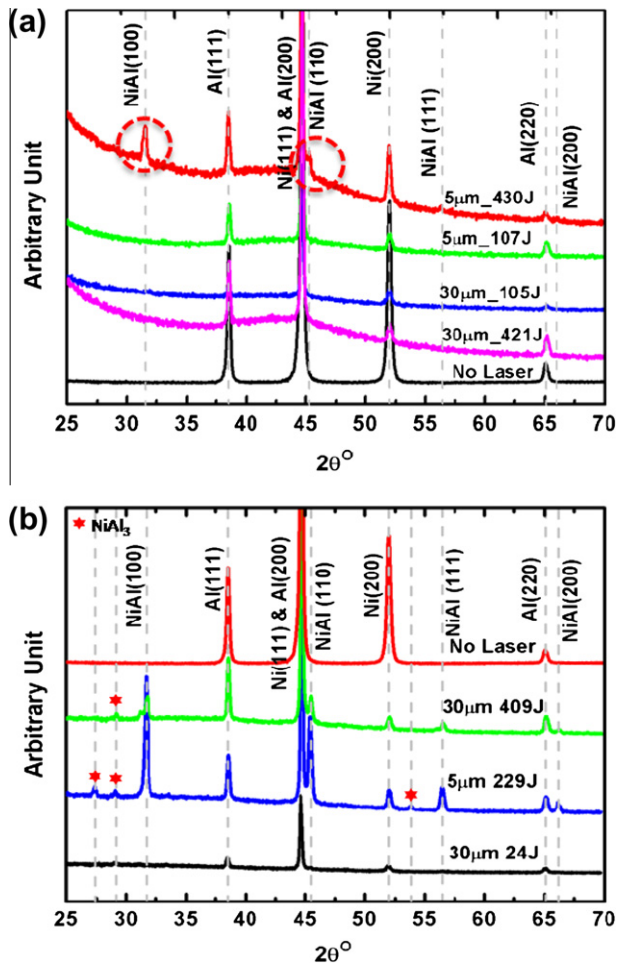

Fig. 9. X-ray diffraction of cross-sectional surfaces of (a) 3 ns and (b) 8 ns laser irradiation. (a) Reaction for 430 J irradiation (5 μm bilayer), represented by circles. (b) Reaction from 229 to 409 J and both 5 and 30 μm bilayer thickness. $NiAl_3$ intermetallic compound was marked by stars.

have more closely spaced Al–Ni interfaces. This evidence proves that bilayer thickness is a significant factor for laser shock-induced reactions. It is also coincident with the conclusions by Ma et al. [52] and Gavens et al. [14], who proved that bilayer thickness of the sample is one of the dominant factors for the exothermic reaction.

By increasing the pulse duration from 3 to 8 ns, the laser intensity was significantly decreased; however, there were more intermetallics found on the irradiated surface, even at the lower laser energies for the thicker bilayer samples as shown in Section 3.3.2. This implies that longer pulse duration can help reactants to overcome the energy barrier for the reaction and suggests that the threshold for the intermetallic reaction is corresponded to shock durations.

The reflected tensile pulse resulted in the expansion, fracture, plastic flow and convex region in the spall. However, the drastic decrease of the shock pressure propagating in the laminates (as shown in Section 3.1) and the energy dissipation on the irradiated surfaces caused by the strong vaporizing, and melting phenomena (see Figs. 5a and c, 6a and c, and 7a, c and e) may significantly attenuate the residual laser-shock energy and result in a lack of intermetallic phase in the spall areas. This also corresponds to the observations in the fragments (Section 4.1).

4.3. Diffusion model

The cross-sectional observations of the recovered samples show a clear distinction of intermetallic formation between the center and the edge of the crater (Fig. 8a–d). This suggests that the shock-induced reactions played an important role in the intermetallic formation. A solid-state diffusion calculation was applied for clarifying the impact of the thermal reaction mechanisms in the Ni/Al laminates. We assume that the reaction was controlled by diffusion and that the temperature is higher than the melting point of Ni (1728 K) and Al (933 K) at ambient pressure due to the severe molten pools on the laser-exposed surface shown in Fig. 8a and b. The total cooling time required for forming the dendrites can be obtained by using a solid diffusion equation. It is postulated that the diffusion takes place primarily at 2000 K, which is higher than the NiAl eutectic point, 1911 K [53]. The self-diffusion coefficients of Ni and Al ($D^*_{Ni} = 1.5 \times 10^{-8}\ cm^2\ s^{-1}$ and $D^*_{Al} = 4.1 \times 10^{-8}\ cm^2\ s^{-1}$ at 2000 K) were obtained from Li et al. [54]. The interdiffusion coefficient, $\tilde{D}$, can be estimated by incorporating the self-diffusion coefficients into Darken's equation:

$$\tilde{D} = N_{Al} D^*_{Ni} + N_{Ni} D^*_{Al} \quad (3)$$

where the N_{Al} and N_{Ni} represent the concentrations of Al and Ni, which are assumed to be equal to 0.5. The estimated interdiffusion coefficient is $2.8 \times 10^{-8}\ cm^2\ s^{-1}$. If there is no reaction barrier (diffusion-controlled reaction), and the diffusion length, l, is taken as the length of the dendrite, 2–3 μm (measured from Fig. 8a and c), then the total cooling time, t, can be obtained from:

$$l = 2\sqrt{\tilde{D}t} \quad (4)$$

It is ~0.25–0.8 s. It should be noted that the temperature of the diffusion process might be lower than 1728 K considering that the dendrites can still be found at ~45 μm in depth from the irradiated surface, where the bilayer maintained a well-defined structure, and no melting of Ni was found. The total cooling time can be much longer than 0.8 s, inasmuch as the temperature might be much lower than 1728 K.

At the edge of the crater, Fig. 8b and d, severe melting was also found, confirming that the temperature was indeed higher than the melting points of Ni and Al. If one assumes that the cooling time is about 0.8 s and the temperature is lower but close to the NiAl eutectic temperature (1900 K), then by a similar calculation (with the self-diffusion coefficients of Ni and Al equal to $2.06 \times 10^{-9}\ cm^2\ s^{-1}$ and $1.5 \times 10^{-8}\ cm^2\ s^{-1}$ [54] at 1900 K), the dendritic length is about ~2 μm. As previously mentioned, the total cooling time might be longer than 0.8 s, and therefore dendrites can be larger than

2 μm. However, no dendrite is seen in Fig. 8b and d. This result suggests that the diffusion-controlled reaction is not the dominant mechanism of the intermetallic reaction in the high energy/short pulse laser irradiation experiments. This implies that the cooling rate is far faster than the required diffusion time and it is more probable to interpret the intermetallic growth by incorporating the shock-induced reaction mechanism due to its rapid reaction (10^7–10^9 faster than diffusion [46]). Nonetheless, it is interesting that Fig. 8d, for the 30 μm bilayer shocked at 400 J, 8 ns, shows a small amount of intermetallics, which have a dendrite length about 1 μm, and no expelled intermetallic phase as shown in Meyers et al.'s [46] and Vecchio et al.'s work [47]. The size of the dendrites seems more consistent with the prediction from the solid diffusion equations. This character provides significant evidence of the effect of the shock-assisted reaction on the thicker bilayer sample irradiated by 8 ns pulse duration laser (400 J). It can be concluded that shock-induced reactions play an important role in both 3 and 8 ns laser shock experiments; however, shock-assisted reaction gains significance as the laser pulse duration increases to 8 ns.

4.4. Reaction propagation

The intermetallic compounds grow as dendrites and propagate to a depth of 50 μm in the 5 μm bilayer shocked at 400 J, 3 ns (Fig. 7a). By using the secondary dendrite arm spacing (SDAS), one can evaluate the cooling rate after laser irradiation and the total cooling time for the reaction products. The equation employed by Masaki et al. [55] is:

$$\lambda \times \left(\frac{dT}{dt}\right)^{\frac{1}{3}} = \mathrm{k} \tag{5}$$

where λ is the secondary dendrite arm spacing (which is about 0.6 μm as measured from Fig. 7), T is the temperature (K), and t is time (s). One can reasonably assume that the value of the constant k is equal to 50 μm $(\mathrm{K\ s^{-1}})^{1/3}$ for Al [56]; hence the cooling rate can be obtained as 5.7×10^5 $(\mathrm{K\ s^{-1}})$. Chvorinov's rule [56] was employed to evaluate the total cooling time after the laser experiment:

$$\dot{\lambda} = k \times t_s^m \tag{6}$$

where k is equal to 8 μm/s^m, m is equal to 5/12 for Al alloys, and t_s represents the total cooling time. The total cooling time was obtained as $t_s = 2.1$ ms and the variation of temperature was estimated as $\Delta T = t_s \times \frac{dT}{dt} \approx 1197$ K. A rational approximation of the highest temperature for the 400 J, 3 ns laser experiment is 1495 K, which is much higher than the temperature at which the intermetallic compounds $NiAl_3$ (1127 K), and Ni_2Al_3 (1406 K) are formed; nevertheless, the temperature is insufficient to melt NiAl (1911 K) and it must therefore form in the solid state, as shown in Fig. 8e. The temperature is sufficient to generate the intermetallic reaction for $NiAl_3$ and Ni_2Al_3 spontaneously, if the reaction time is adequate for the thermal diffusion process. This explains why the increase in pulse duration introduces other intermetallic phases ($NiAl_3$) in the recovered sample.

5. Conclusions

Shock compression and spalling of Ni–Al laminates with two different bilayer thicknesses (5 and 30 μm) was carried out at laser energies between ~24 and ~400 J, and with pulse durations of 3 and 8 ns. The following principal conclusions were reached:

1. The laser shock created craters, spall, and also extreme damage in all laminates.
2. The laser energies were insufficient to generate self-propagating reaction through the entire samples; however, the shock-induced reactions produced intermetallic reactions to ~50 μm of depth from the irradiated surface using 400 J, 3 ns laser shock.
3. The bilayer thickness is an important geometrical factor for laser shock-induced reactions. Thinner Ni–Al bilayers (5 μm) demonstrate sub-critical/critical behavior forming molten Al and Ni–Al compounds, whereas thicker bilayers do not exhibit significant reaction.
4. The shock-assisted thermal reaction mode is a significant mechanism in the experiments with 8 ns laser pulse duration.
5. The reacted regions showed dendritic structures, from which the secondary dendrite arm spacing could be measured. This enabled the estimation of the cooling rate, $\sim 5.7 \times 10^5\ \mathrm{K\ s^{-1}}$ and cooling time, 2.1 μs. The total temperature rise, ΔT, is about ~1200 K.
6. Laser pulse duration is an important factor for obtaining reactions in both thinner and thicker bilayer samples under relatively low laser intensity because of the increase of the thermal heating time for the longer laser pulse duration (3 vs. 8 ns).

Acknowledgements

Funding was provided by Grant ONR MURI N00014-07-1-0740 and ILSA Contract No. W-7405-Eng-48. The help provided by Dr. D. Correll is gratefully acknowledged. The authors greatly appreciate the generous help from Prof. Gustaf Arrhenius and Saul Perez-Montano at Scripps Institution of Oceanography, in conducting XRD analysis and from Drs. Tilllack and Larsen, in supplying us with HYADES code. The authors also thank Calit2's Nano3 Lab and Scripps Institute of Oceanography for access to the SEM.

References

[1] Thadhani NN. Prog Mater Sci 1993;37:117.
[2] Eakins DE, Thadhani NN. Intl Mat Rev 2009;54:118.

[3] Nesterenko VF, Meyers MA, Chen HC, LaSalvia JC. Appl Phys Lett 1994;65:3069.
[4] Nesterenko VF, Meyers MA, Chen CH, LaSalvia JC. Metall Mater Trans A 1995;26A:2511.
[5] Chen HC, LaSalvia JC, Nesterenko VF, Meyers MA. Acta Mater 1998;46:3033.
[6] Chen HC, Nesterenko VF, Meyers MA. J Appl Phys 1998;84:3098.
[7] Batsanov SS. Effects of explosions on materials: modification and synthesis under high-pressure shock compression. New York: Springer-Verlag; 1994.
[8] Wang J, Besnoin E, Duckham A, Spey SJ, Reiss ME, Knio OM, et al. J Appl Phys 2004;95:248.
[9] Wang J, Besnoin E, Knio OM, Weihs TP. Acta Mater 2004;52:5265.
[10] Swiston AJ, Hufnagel TC, Weihs TP. Scripta Mater 2003;48:1575.
[11] Duckham A, Spey SJ, Wang J, Reiss ME, Besnoin E, Knio OM, et al. J Appl Phys 2004;96:2336.
[12] Wang J, Besnoin E, Duckham A, Spey SJ, Reiss ME, Kino OM, et al. Appl Phys Lett 2003;83:3987.
[13] Reactive Nano Technologies, Inc. Applications <www.rntfoil.com/site/applications>.
[14] Gavens AJ, Heerden DV, Mann AB, Reiss ME, Weihs TP. J Appl Phys 2000;87:1255.
[15] Blobaum KJ, Heerden DV, Gavens AJ, Weihs TP. Acta Mater 2003;51:3871.
[16] Horie Y, Graham RA, Simonsen IK. Mater Lett 1985;3:354.
[17] Simonsen IK, Horie Y, Graham RA, Carr MJ. Mater Lett 1987;5:75.
[18] Miracle DB. Acta Metal Mater 1993;41:649.
[19] Ansara I, Dupin N, Lukas HL, Sundman B. J Alloys Compd 1997;247:20.
[20] Dong S, Hou P, Yang H, Zou G. Intermetallics 2002;10:217.
[21] McQueen RG, Marsh SP. J Appl Phys 1962;33:654.
[22] Vidal F, Johnston TW, Laville S, Barthélemy O, Chaker M, Le Drogoff B, et al. Phys Rev Lett 2001;86:2573.
[23] Kanel GI, Fortov VE. Adv Mech 1987;10:3.
[24] Rosenberg Z, Luttwak G, Yeshurun Y, Partom Y. J Appl Phys 1983;54:2147.
[25] Chen D, He H, Jing F. J Appl Phys 2007;102:033519.
[26] Andriot P, Chapron P, Lambert V, Olive F. Shock waves in condensed matter. Amsterdam: Elsevier Science; 1983.
[27] Rybakov AP, Rybakov IA. Mech Eur J B Fluids 1995;14:197.
[28] Zhiembetov AK, Mikhaylov AL, Smirnov GS. AIP Conf Proc 2002;620:547.
[29] Holtkamp DB, Clark DA, Garcia IA. AIP Conf Proc 2004;705:473.
[30] Holtkamp DB, Clark DA, Garcia IA. AIP Conf Proc 2004;705:477.
[31] Schneider MS, Kad BK, Gregori F, Kalantar DH, Remington BA, Meyers MA. Int J Impact Eng 2005;32:473.
[32] Wei CT, Maddox BR, Weihs TP, Stover AK, Nesterenko VF, Meyers MA. API Conf Proc 2009;1195:305.
[33] Kim JS, LaGrange T, Reed BW, Taheri ML, Armstrong MR, King WE, et al. Science 2008;321:1472.
[34] Jarmakani HN, Bringa EM, Earhart P, Remington BA, Nhon V, Meyers MA. Acta Mater 2008;56:5584.
[35] Cao B, Bringa EM, Meyers MA. Met Mater Trans A 2007;38:2681.
[36] Jarmakani H, Maddox B, Wei CT, Kalantar D, Meyers MA. Acta Mater 2010;58:4604.
[37] Stover AK, Walker NK, Knepper R, Fritz GM, Hufnagel TC, Weihs TP. Correlating mechanical properties to microstructure in rolled nickel aluminum reactive laminates. Boston: JANNAF Conference; 2008.
[38] Lindl J. Phys Plasmas 1995;2:3933.
[39] Samsonov GV. Handbook of the physicochemical properties of the elements. New York: Washington; 1968.
[40] Meyers MA. Dynamic behavior of materials. 2nd ed. New York: Wiley; 1994.
[41] Nesterenko VF. Dynamics of heterogeneous materials. New York: Springer-Verlag; 2001.
[42] Eakins DE, Thadhani NN. Mater Res Soc Symp Proc 2006;896:0896-H06-04.1.
[43] Jarmakani H, Maddox BR, Wei CT, Kalantar D, Koniges A, Eder D, et al. Acta Mater 2010;55:4604.
[44] Vitali E, Wei CT, Benson DJ, Meyers MA. Acta Mater 2011.
[45] Sagel A, Sieber H, Fecht H-J, Perepezko JH. Acta Mater 1998;46:42333.
[46] Meyers MA, Yu L-H, Vecchio KS. Acta Metall Mater 1994;42:715.
[47] Vecchio KS, Yu L-H, Meyers MA. Acta Metall Mater 1994;42:701.
[48] KoČi L, Bringa EM, Ivanov DS, Hawreliak I, McNaney J, Higginbotham A, et al. Phys Rev B 2006;74:012101.
[49] Boehler R, Ross M. Earth Planet Sci Lett 1997;153:223.
[50] Trenkle JC, Weihs TP, Hufnagel TC. JANNAF Conference Proceeding; 2008.
[51] Trenkle JC, Koerner LJ, Tate MW, Gruner SM, Weihs TP, Hufnagel TC. App Phys Lett 2008;92:081903.
[52] Ma E, Thompson CV, Clevenger LA, Tu KN. Appl Phys Lett 1990;57:1262.
[53] Okamoto H. J Phase Equilibria 1993;14:257.
[54] Li GX, Liu CS, Zhu ZG. Phys Rev Lett 2005;71:094209.
[55] Masaki Y, Wei-Feng Q, Suzuki M, Kitagawa A. Japn J Appl Phys 1994;33:1019.
[56] Askeland DR, Fulay PP. The science and engineering of materials. 4th ed. Tampa: Thompson; 2005.